

Field Observations of the Electromagnetic Properties of First-Year Sea Ice

Donald K. Perovich, Jacob Longacre, David G. Barber, Robert A. Maffione, Glenn F. Cota, Curtis D. Mobley, Anthony J. Gow, Robert G. Onstott, *Member, IEEE*, Thomas C. Grenfell, *Associate Member, IEEE*, W. Scott Pegau, Mark Landry, and Collin S. Roesler

Abstract—An interdisciplinary field experiment was conducted during April and May of 1994 at Point Barrow, AK, to investigate the relationship between the electromagnetic and physical-biological properties of first-year sea ice. Electromagnetic signatures of bare and snow-covered first-year ice were measured over a broad spectral range, including ultraviolet through near-infrared albedo, microwave emissivity, and radar backscatter. Observations indicated that the scattering of visible light varied significantly with depth in response to changes in the size and orientation of the ice crystals and in the number of brine and air inclusions. The scattering of visible light was greatest in the surface layer where there were numerous inclusions, and crystals tended to be small and randomly oriented. Changes in albedo over small horizontal distances were found to be related to surface layer conditions, including the number of air bubbles and particulate levels. Even for bare ice, transmittances were small with peaks in the blue-green. Scattering exceeds absorption throughout the snow and ice except in the skeletal layer colonized by bottom ice algae. Passive microwave emissivities showed a substantial difference between snow-covered and snow-free sites due to the effects of impedance matching at lower frequencies and volume scattering at higher frequencies produced by the snow. Spatial variability in the emissivity was quite small except at 90 GHz, where the emissivity was most sensitive to the amount of depth hoar. Radar backscatter coefficients were 5–6 dB larger for oblique viewing angles over snow-covered ice.

Index Terms—Electromagnetic properties, physical-biological properties, remote sensing, sea ice, snow cover.

Manuscript received November 11, 1997; revised May 25, 1998. This work was supported by the Office of Naval Research as part of an accelerated research initiative on the electromagnetic properties of sea ice.

D. K. Perovich and A. J. Gow are with the U.S. Army Cold Regions Research and Engineering Laboratory, Hanover, NH 03755 USA (e-mail: tgow@crrel.usace.army.mil).

J. Longacre and M. Landry are with the Naval Undersea Warfare Center, New London, CT 06320 USA.

D. G. Barber is with the Centre for Earth Observation Science, Department of Geography, University of Manitoba, Winnipeg, Man., R3T 2N2 Canada.

R. A. Maffione is with HOBILabs, Inc., Watsonville, CA 95076 USA.

G. F. Cota is with the Center for Coastal Physical Oceanography, Old Dominion University, Norfolk, VA 23508 USA.

C. D. Mobley is with Sequoia Scientific, Inc., Mercer Island, WA 98040 USA.

R. G. Onstott is with the Environmental Research Institute of Michigan, Ann Arbor, MI 48107 USA.

T. C. Grenfell is with the Department of Atmospheric Sciences, University of Washington, Seattle, WA 98195 USA.

W. S. Pegau is with Oregon State University, Corvallis, OR 97331 USA.

C. S. Roesler is with the Department of Marine Sciences, University of Connecticut, Groton, CT 06340 USA.

Publisher Item Identifier S 0196-2892(98)06757-6.

I. INTRODUCTION

SATELLITE remote-sensing data, especially at microwave frequencies, offer a powerful tool for studying the large-scale geophysics of sea ice. In addition, the absorption, reflection, and transmission of visible and infrared radiation by ice are fundamental processes governing ice thermodynamics and biological productivity beneath the ice. It is important to understand the electromagnetic properties of sea ice over a wide range of frequencies. Achieving such an understanding is complicated by the highly variable nature of the electromagnetic signatures of sea ice. Sea ice is a complex composite of ice, brine, solid salts, and air that is near, or at, its melting point with biogenic and lithogenic particulate inclusions. Because of this, there is significant variability in the physical state and structure of the ice, which in turn causes variability in the electromagnetic properties of the ice [1], [2].

The Office of Naval Research, Arlington, VA, sponsored a research initiative designed to relate the physical and electromagnetic properties of sea ice and develop forward and inverse models of sea ice electromagnetic properties [3]. In this initiative, an interdisciplinary approach was strongly emphasized that combined ice physical properties with electromagnetic properties: optics with microwave, physics with biology, and observations with theory. Laboratory experiments, in which greater control could be exerted on ice properties and environmental conditions, were a central element in this initiative. However, for all of the strengths of the laboratory studies [4], there were limitations. For example, only thin ice (<0.5 m) could be studied. To supplement the laboratory studies, a field program was conducted during April and May of 1994 at Point Barrow, AK. The field program had two general goals, as follows.

- Extend the laboratory work to include thick first-year ice.
- Add new experimental techniques and investigate phenomena that cannot be studied in the laboratory, such as the impact of sea ice biota on electromagnetic properties.

As was the case for the laboratory work, a collaborative, interdisciplinary approach was used in the field study. The focus of this experiment centered on obtaining a complete description of the physical, biological, and electromagnetic properties of snow-covered and bare first-year sea ice. During this experiment, we measured the electromagnetic signatures of first-year ice over a broad spectral range, including ul-



Fig. 1. Photograph of experimental site. The snow cover has been removed from part of the area so that bare ice as well as snow-covered ice can be studied. Part of the research team is shown measuring radar backscatter, microwave emissivity, ultraviolet transmission, and visible transmittance over bare ice.

traviolet, visible and near-infrared albedo and transmittance, microwave emissivity, and radar backscatter. In addition, the small-scale variability of these signatures was examined. The effect of the snow cover on electromagnetic signatures was determined by comparing snow-covered and bare ice signatures. Profiles of optical properties within the ice were determined, and the impact of ice platelet orientation on light scattering was investigated. In this paper, we explain the varied techniques and instruments used in the field experiment and present an overview of representative results from the study.

II. INSTRUMENTS AND METHODS

The field operations were based at the National Arctic Research Laboratory, Point Barrow. The observation site was located approximately 0.5 km offshore of Point Barrow in the Beaufort Sea. Here we studied undeformed, 1.75-m-thick first-year ice that began growing in November 1993. Measurements commenced May 1 and continued through May 8. On May 5, the snow cover was removed from half of the experimental area and measurements of the bare ice were made. The key to the experiment was in making coordinated, integrated measurements to obtain a complete electromagnetic and physical description of the snow and ice. To facilitate this, a 20×10 -m rectangle was selected as the location for group measurements (Fig. 1). A team of 20 researchers worked in this area, measuring the physical, biological, optical, and microwave properties of the snow and ice. Fig. 1 shows the experimental site and gives an indication of both the variety and integration of the measurement program. Pictured are members of the research team measuring radar backscatter, microwave emissivity, ultraviolet transmission, and visible transmittance for bare ice.

A. Snow and Ice Physical Properties

The physical properties of the snow cover were sampled coincidentally with electromagnetic observations. Snowpit depths were recorded to the nearest half centimeter with a meter stick. Density samples were removed at 2-cm vertical intervals with a 66.36-cm^3 snow sampler, placed into a sealed plastic bag, and weighed to the nearest tenth of a gram on a digital scale. We estimate the precision of this approach to be within $\pm 40\text{ kg}\cdot\text{m}^{-3}$ [5]. Snow salinity and ice surface salinity were measured from melted samples using a refractometer, precise to 1 ppt. Snow grains were photographed using a 35-mm camera and 60-mm micro lens. These photographs were then digitized into a microcomputer, where an operator defined individual grains. Snow grain morphological parameters, including area, perimeter length, and major and minor axis of a best-fit ellipse, were automatically computed and output to a database [5].

Salinity, density, and *in situ* temperature measurements were used to compute the partial fractions of ice, brine, and air within the snow volume. The relative proportions of each are important in modeling the complex dielectric constant of the material and in defining the thermodynamic properties of the volume. Brine volumes were computed from tables developed by Assur [6] and later converted to equations by Frankenstein and Garner [7].

Vertical profiles of ice temperature, salinity, and density were determined from ice cores. The Cox and Weeks [8] relationships were used to determine brine and air volumes from measurements of ice salinity, temperature, and density. The ice crystal structure was identified from vertical and horizontal thin sections [2], [9]. These thin sections were also used to determine number density and inclusion size distributions of brine pockets in the ice. Snow samples and 5–10-cm-long sections of the ice cores were melted and

processed to determine particulate (GF/F filter collections) and dissolved (filter passing) absorption coefficients spectrophotometrically [10]–[13]. Particle composition, concentration, and size distribution were determined using a Galai CIS100 Particle Analyzer with a charge coupled device (CCD) video camera display [14], [15]. Chlorophyll and algal pigment concentrations were measured fluorometrically [16] and spectrophotometrically, respectively.

B. Optical Properties

Spectral and wavelength-integrated albedos and spectral transmittances were measured for the bare and snow-covered cases. Visible and near-infrared measurements were made using two instruments: a Spectron Engineering SE-590 and an Analytical Spectral Devices ASD-PS II. Both instruments use a diffraction grating and a photodiode array to cover the range from 400 to 1000 nm [17]. Two Kipp radiometers were used to measure all-wave (300–3000 nm) incident and reflected irradiance. A LI-COR quantum sensor LI-190SA was used to measure incident photosynthetically active radiation (PAR, 400–700 nm) and for corrections of incident flux. Ultraviolet measurements were made at 308, 320, 340, and 380 nm, using a Biospherical Instruments PUV-500 ultraviolet radiometer.

A typical measurement sequence consisted of measuring incident and reflected irradiances with the above-ice detectors, then submerging the under-ice detectors to measure transmitted irradiance or radiance. The under-ice units were mounted on a 1.0–1.3-m-long articulated arm that allowed ice away from the hole to be sampled. Underwater radiance was converted to irradiance by multiplying by 3.14, which assumes an isotropic light field. The ultraviolet instrument had a separate underwater detector, while the SE-590 detector was mounted in a waterproof housing, allowing it to be placed under the ice. The ASD sensor with its submersible fiber-optics probe was mounted in a serrated scraper cup. One spectra was collected below the ice algal layer followed by another above after scraping the algal layer off. Spectral albedos [$\alpha(\lambda)$] were calculated from the ratio of the measured reflected [$E_r(\lambda)$] and incident [$E_d(\lambda)$] spectral irradiance

$$\alpha(\lambda) = \frac{E_r(\lambda)}{E_d(\lambda)}.$$

Spectral transmittances [$T(\lambda)$] were determined from the ratio of the transmitted irradiance at the bottom of the ice ($z = H$) to the incident irradiance on the surface ($z = 0$)

$$T(\lambda) = \frac{E_d(\lambda, H)}{E_d(\lambda, 0)}.$$

New techniques were applied in this experiment to measure the irradiance attenuation coefficient (K), beam spread function (bsf), and the transmitted beam profile within the ice column. Vertical profiles of spectral radiance within the ice were measured using an instrument designed by WET Labs, Inc., using a 13-cm-diameter diffusing sphere. This sphere was enclosed between two 14-cm-diameter light shields that prevented the

globe from measuring light along the axis of the hole, giving an azimuthally averaged irradiance heavily weighted toward the horizontal direction. Because of the design of the optical instrumentation, shadows and rapid changes in the light field have a strong influence on measurements made near the ice surface (upper 25 cm). Irradiance attenuation coefficients [$K(\lambda, z)$] were calculated as the slope of a linear regression of the natural log of radiance versus depth

$$K_L(\lambda, z) = \frac{d\{\ln[L(\theta, \phi, \lambda, z)]\}}{dz}.$$

The instrument used to measure the bsf consisted of two canisters, one containing a laser diode source (670 nm) and the other an irradiance detector [18]. Two parallel holes were cored in the ice with a separation R using a specially engineered ice corer. The source canister was lowered into one of the holes to a particular depth with the light source aimed toward a second hole. The detector was then slowly lowered into the second hole, with the detector aimed toward the source, until a peak signal was received, indicating source and receiver alignment. Measurements were recorded continuously. The source was then held at a fixed depth and rotated approximately 10° , either clockwise or counterclockwise, and held in that position until 25–50 measurements were recorded by the phase-synchronized detector. Subsequent measurements were made by sequentially rotating the source at increments of 10° . Once the complete bsf was measured, the source depth was changed, the receiver realigned with the source, and the measurement process repeated.

Measurements of the beam profile of light transmitted through sea ice were also made. The optical source was a frequency doubled, pulsed, diode-pumped 523-nm Neodymium YLF laser (20 mJ/pulse, 2-kW peak power, 20-mW average power). Light from this laser was shone downward into the ice, while a detector placed under the ice was moved horizontally to determine transmitted radiance as a function of distance from the center beam position. The effect of ice thickness was investigated by drilling holes of various depths and placing the source at the bottom of each hole and repeating the transmission observations.

C. Microwave Properties

The passive microwave observations specifically included horizontal polarization (H-pol) and vertical polarization (V-pol) measurements of brightness temperature and emissivity at microwave frequencies of 6.7, 10, 19, 37, and 90 GHz. These measurements were made at a nadir angle of 50° . Simultaneous broad-band measurements were made in the thermal infrared (8–14 μm) to determine ice skin temperature and infrared emissivity. The radiometers were mounted on a sled, and measurements were made at selected sites and along horizontal traverses.

Active microwave and millimeter-wave properties were measured using a radar polarimeter. Instruments operating in six bands between 0.5 and 95 GHz were used, each with a typical operating bandwidth less than 2 GHz. The radar

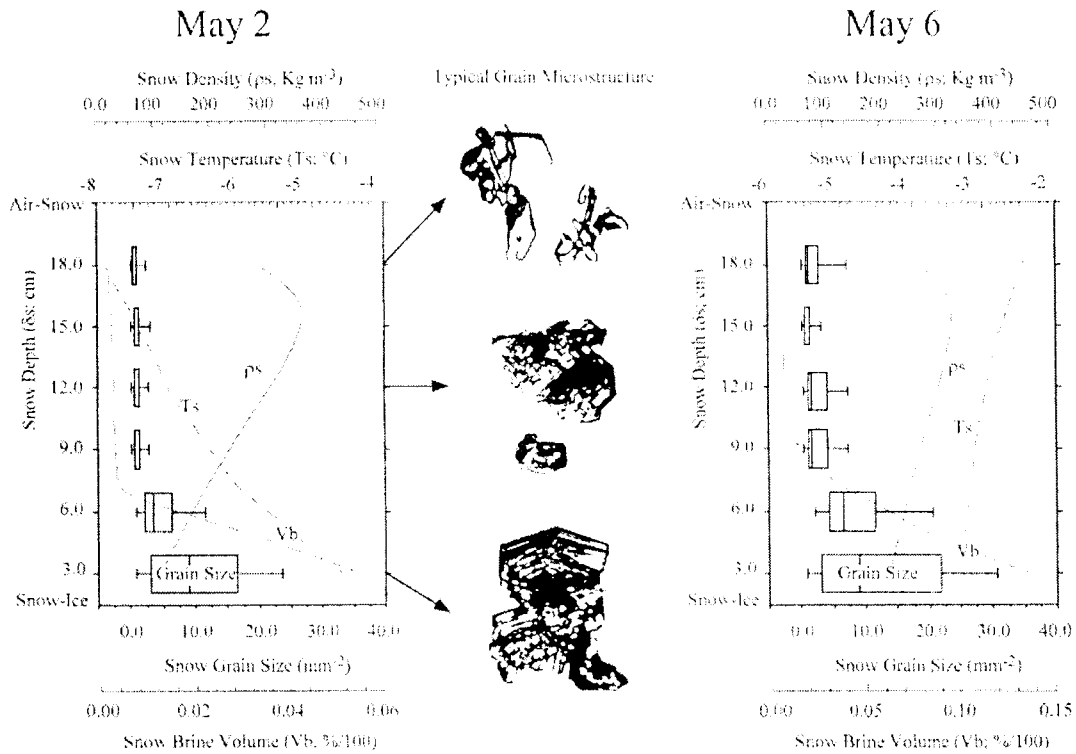


Fig. 2. Snow physical properties as a function of depth on May 2 and May 6. Snow temperature, density, brine content, and grain size are plotted. Photographs showing snow grain microstructure are also presented.

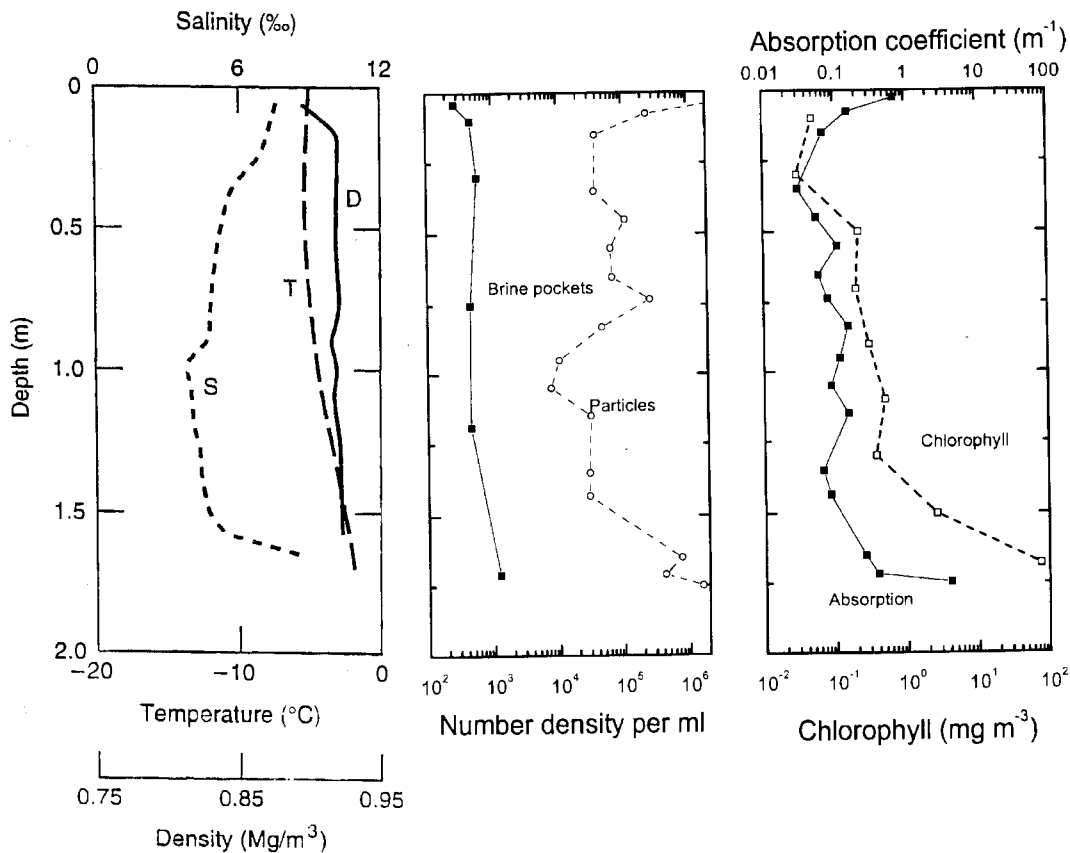


Fig. 3. Vertical profiles of ice salinity, temperature, and density; the number density of brine pockets and particles; and chlorophyll concentration; absorption coefficients of the particulate and dissolved material (400 nm) [m^{-1}] and chlorophyll concentration [$mg\ m^{-3}$].

was operated in the monostatic mode, where the transmit and receive antennas were collocated. Linear polarization was used, creating a complex matrix to describe scattering at VV-, VH-, HV-, and HH-polarizations. The first letter denotes the transmit polarization, while the second denotes the received polarization. The radar antenna arrays were mounted on a sled and positioned at a height of about 3 m above the ice surface.

III. RESULTS AND DISCUSSION

A. Physical Properties

The snow physical and electrical properties measured during the field experiment are representative of the transitional period between winter and the onset of melt. Most of the snow cover consisted of windpacked snow, with a 1-cm layer of new loose snow on the surface and a 2-cm-thick basal layer, kinetic growth grains. Although there was little if no water in liquid phase within the snow cover during this period, the metamorphism within the snow pack was proceeding rapidly under temperature gradient metamorphism. Close examination of the evolution of the snow cover in this type of snow pack shows that the basal layer consisted of faceted and cupped-shaped grains (Fig. 2). This high-salinity, low-density layer merges into an increasingly dense vertical profile. The lower density layer at the surface evidenced recent snow deposition. The temperatures fluctuated between a relatively strong gradient (May 2, 1994) to a more isothermal state (May 6, 1994). Under the temperature gradient conditions, the basal grains grew through kinetic growth processes, resulting in anisotropically aligned grains (long axis aligned with the vapor pressure gradient). Grains in the center of the pack were rounder in shape and of high density due to cold temperature saltation over the winter period. New snow at the surface was very fine-grained with small facets remaining from the precipitation crystal structure. This three-layer snow system is typical of natural snow conditions on first-year sea ice [5]. In addition, an accumulation of particles (1900 ml^{-1}) was observed in the basal snow layer. These particles were associated with an absorption coefficient of 0.04 m^{-1} at 400 nm , which decayed exponentially with wavelength. This absorption would result in enhanced heating within the snow layer.

As the atmospheric temperatures warmed between May 2 and 6, we observed an increase in the snow grain size at most of the levels within the snow pack (Fig. 2). This growth was due to equitemperature metamorphism, in which larger grains grow at the expense of smaller ones. In the basal layer, the presence of significant volumes of brine tended to break down the sharp-edged kinetic growth grains into large, more rounded shapes. We noted that the brine volume responded very strongly to the increasing temperature within the basal layer, substantially increasing the effective complex permittivity within the snow basal layer and at the ice surface. This thermodynamic relationship and the contrast between laboratory and field conditions of the snow cover are examined elsewhere in this issue [19].

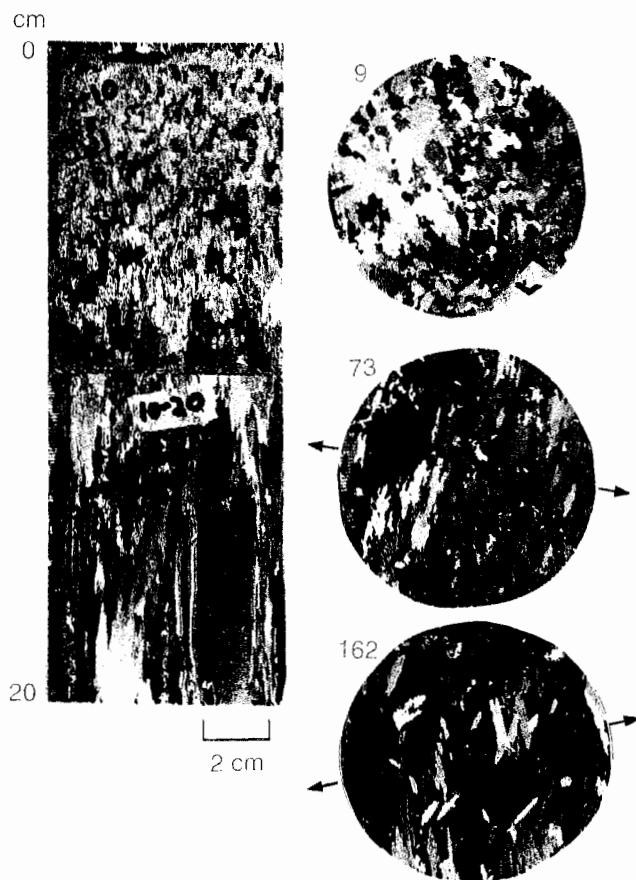


Fig. 4. Vertical and horizontal thin section photographs of the ice cover. The scale of the photographs and the c -axis alignment of the crystals are indicated in the figure.

The ice was 1.65–1.75 m thick and had formed during a single uninterrupted episode of freezing. Spring warming of the ice cover was evident, with temperatures in the upper 0.5 m of the ice approximately -5.5°C (Fig. 3). Temperatures increased linearly with depth. Ice salinities reflected the typical c -shaped profile of first-year ice with values ranging from 7–9 o/oo near the surface to 4–5 o/oo for the bulk of the interior and increasing to 10 o/oo near the bottom. Brine volumes were in the 5–12% range. Air volumes were about 4% in the upper 10 cm of the ice cover, but less than 1% in the remainder of the ice.

Since the electromagnetic properties of sea ice are affected not only by the volume of brine, but by how the brine is distributed [20], we measured the number density and size of the brine inclusions. The brine pocket number density ranged from 1 to 2 inclusions mm^{-3} for most of the ice cover, with median cross-sectional areas of 0.01 – 0.02 mm^2 .

In addition to the brine pockets, particles, including bacteria and chlorophyll-rich algae, were present in the ice. Optically, these particles are weak scatterers and potentially strong absorbers. Particle concentrations were highest near the top and bottom of the ice cover (10^6 ml^{-1}) and a factor of 10–100 smaller in the interior of the ice (Fig. 3). The high particle concentrations near the surface were due primarily to

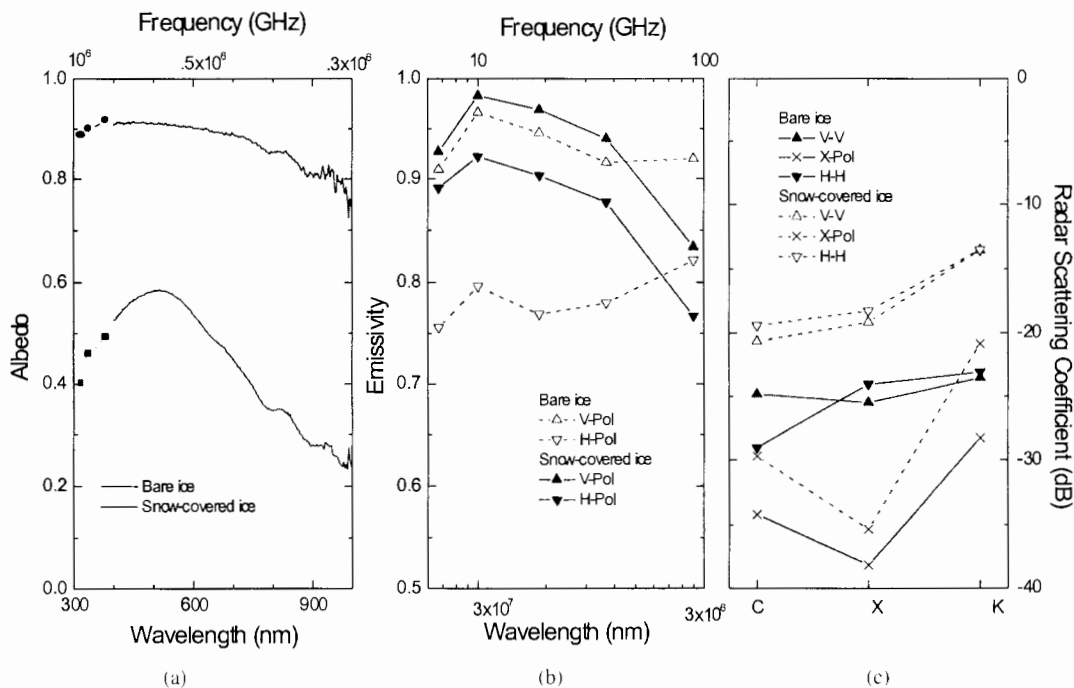


Fig. 5. Electromagnetic signatures of snow-covered first-year ice and bare first-year ice showing (a) spectral albedo, (b) emissivity, and (c) radar scattering coefficient.

bacterial cells and marine-derived aggregate organic material entrained in the ice, while those near the bottom were related to the relatively high levels of algae present. While the particle concentrations were large, the modal diameter of the particles was quite small with average diameters of 2–3 μm . Aggregate diameters were approximately 30–50 μm , although the concentrations of these particles were three orders of magnitude less than those of the smaller particles. Chlorophyll concentrations were between 0.1 and 1 mg m^{-3} throughout the ice column, increasing sharply to values greater than 300 mg m^{-3} in the bottom few centimeters of ice.

Structurally, the ice cover consisted completely of columnar congelation ice that included a surface layer of about 10 cm of fine-grained transition ice (Fig. 4). Cores contained abundant banding, attributable to weather-controlled fluctuations of ice growth rates. A very rapid aligning of c-axes was observed at this site. Significant alignments had occurred by 30 cm, increasing to very strong alignments at the bottom of the ice sheet. A slight (10–15°) swing in the c-axis alignment direction near the bottom of the ice sheet was attributed to the effects of nearby pressure ridge formation causing a small change in the direction of the prevailing current, generally paralleling the shoreline.

B. Electromagnetic Signatures

The electromagnetic signatures of the snow-covered and the bare first-year ice are plotted in Fig. 5. These results include spectral albedos from 400 to 1000 nm, emissivity from 6 to 90 GHz, and radar backscatter for C-, X-, and K-band. The passive and active microwave measurements were made at nadir angles of 50 and 45°, respectively. Spectral albedos

were comparable to those reported by earlier researchers [17], [21]–[23]. Values for the snow-covered ice were large and exhibited little spectral dependence. Bare ice albedos were smaller at all wavelengths and varied spectrally by more than a factor of two, decreasing from a peak value of 0.6 at approximately 500 nm to 0.25 at 1000 nm. Removing the snow cover resulted in a decrease in wavelength-integrated albedo from 0.85 to 0.45.

The difference between the emissivity spectra for bare and snow-covered ice is significant. With a snow cover, the emissivity is relatively high and the difference between V-pol and H-pol values is nearly constant. The spectral dependence is a result of the layered structure. At 6.7 GHz, the snow-ice interface layer contributes most strongly. Because its reflectivity is relatively large, the emissivity is lower than at 10 GHz, where the snow layer is more absorbing. This decrease at higher frequencies is due to the influence of volume scattering by the snow grains. For the snow-free case, the emissivity spectra are relatively flat and the difference between V-pol and H-pol is two to three times as large as for the snow-covered case. The behavior for both cases is essentially the same as has been observed in laboratory experiments at the CRREL pond [4].

Radar backscatter values were greater by 5–10 dB for the snow-covered ice than for the bare ice. This was true at all frequencies and all polarizations. These results are consistent with earlier radar studies of snow-covered first-year ice [24]. It is interesting to note that the cross-pol (X-pol) results show a minimum at X-Band. Since X-pol signal was primarily due to multiple scattering, the reduced scattering at X-band implies higher emissivity, lending support to the observed maxima in the emissivity at 10 GHz in the passive microwave results.

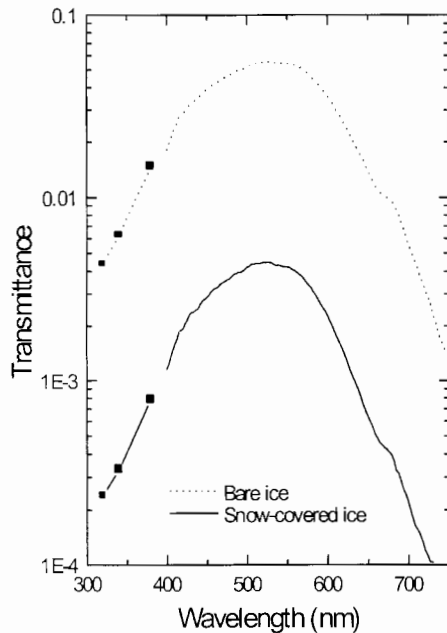


Fig. 6. Spectral transmittance from 300 to 750 nm for snow-covered and bare first-year ice. The snow depth was 0.12 m, and the ice thickness was 1.7 m.

C. Optical Properties of the Total Ice Column

We measured the spectral distribution of the light transmitted through the snow-covered ice. Albedos were high, attenuation was significant, and very little light penetrated through the snow-covered ice. Transmittances were quite small, with a peak value of only 0.005 (i.e., 0.5%) at 500 nm (Fig. 6). Ultraviolet light was strongly attenuated by the snow-covered ice, and transmittances ranged from 0.001 at 380 nm to 0.0002 at 305 nm. Removing the 0.12-m-thick snowcover resulted in an order of magnitude increase in transmittance across the spectrum. For the bare ice, transmittances ranged from a minimum of 0.005 at 305 nm to a maximum of 0.06 near 500 nm. Comparing the two cases plotted in Fig. 6 demonstrates the large impact of snow depth on light transmittance.

The influence of ice algal colonization of sea ice was particularly evident in the skeletal layer where they are most abundant. Fig. 7 shows visible transmittance spectra for bare ice with and without the ice algal layer present and the diffuse attenuation spectra across the bottom ice algal layer. Peak transmittances without the algal layer were 0.073 near 530 nm and decreased to 0.01 at 700 nm. Although the bottom ice algal layer was only about a centimeter thick, there was significant attenuation over that layer. Transmittance maxima with algae present fall to 0.066 and shift slightly toward the red. The spectral attenuation over this layer had a signature characteristic of absorption by algal pigments dominated by diatoms [25]. Chlorophyll *a* absorbs strongly in the blue and red with peaks around 440 and 670 nm. Absorption by carotenoids causes the broad shoulder in the blue-green region of the attenuation spectra. Attenuation in the algal layer was qualitatively proportional to the algal biomass accumulation. Spectrally averaged attenuation coefficients for the algal layer were of the same magnitude as snow and about an order of magnitude greater than uncolonized sea ice.

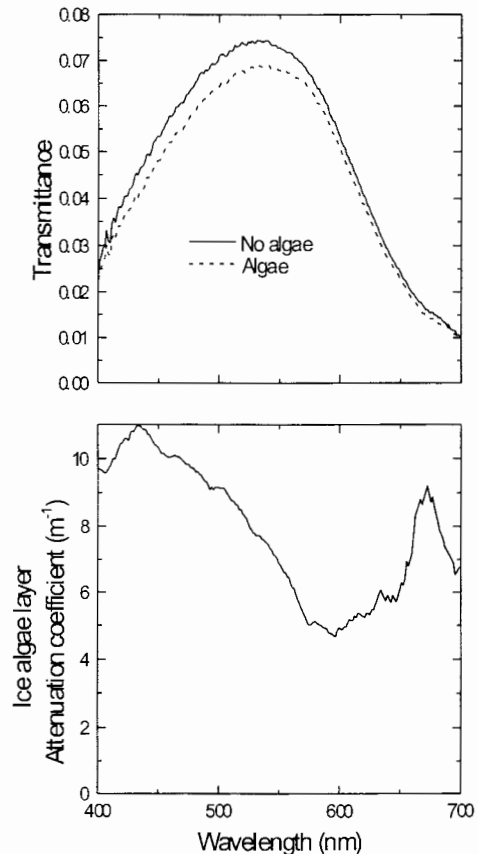


Fig. 7. Effect of a bottomside ice algal layer on visible light transmittance. Top: spectral transmittance with and without algae, and Bottom: spectral attenuation coefficient of the ice algal layer.

D. Profile Optical Properties

The attenuation measurements shown in Fig. 8 were obtained using the in-ice spectral radiometer. Diffuse attenuation coefficients were calculated in intervals of 5 cm along the length of the profile. These data are easiest to interpret once the asymptotic state is reached. In the asymptotic limit, the diffuse attenuation coefficient is independent of the measurement configuration; therefore, this measurement equals the irradiance attenuation coefficient.

Near the surface, the value of $K(665)$ is approximately three times that of $K(461)$. Below 0.5 m, that ratio drops to approximately two. Assuming that the light field is nearly asymptotic below 0.5 m, we find that the attenuation coefficients have a spectral shape similar to that presented by Grenfell and Maykut [21]. However, the magnitude of the attenuation coefficients is about one-third of their value for first-year blue ice. We measured these small attenuation values in the interior of the ice, which was fairly clear, with large-oriented crystals and very few air bubbles. We suspect that scattering was relatively low in the interior, resulting in small attenuation coefficients. Transmittance observations indicated that attenuation coefficients averaged over the entire depth of the ice were roughly three times larger. The implication is that attenuation was much greater in the bubbly surface layer of the ice and near the bottom where there were significant algal concentrations. Profile measurements in these regions are needed.

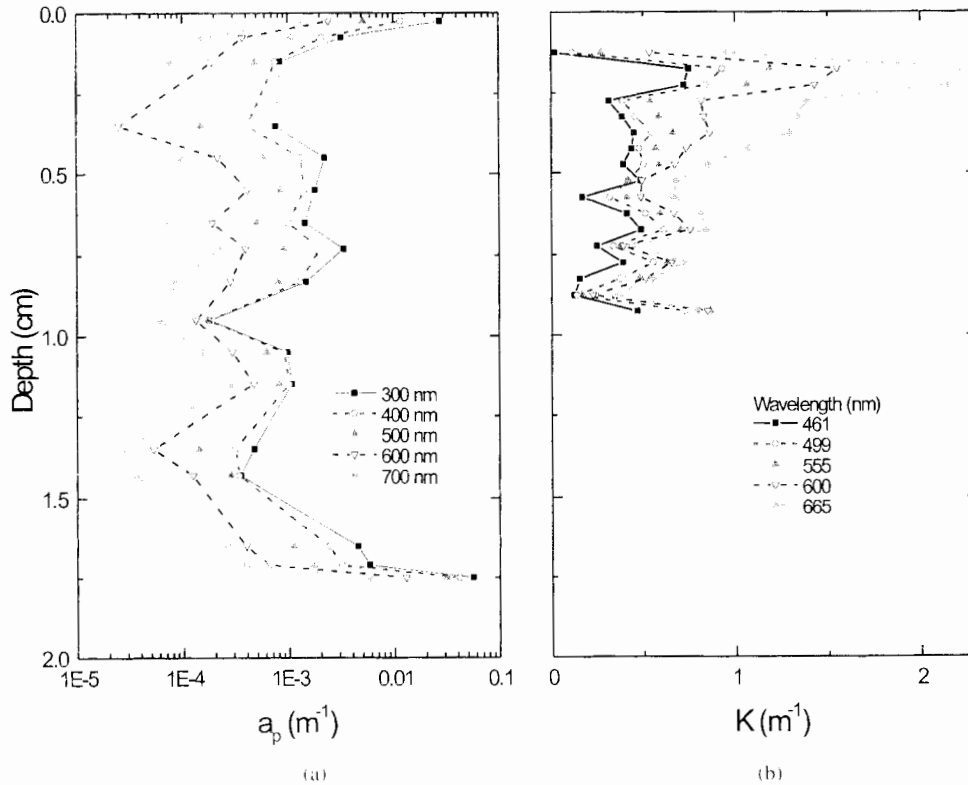


Fig. 8. Vertical profiles at selected wavelengths of (a) particulate absorption coefficient and (b) diffuse attenuation coefficient.

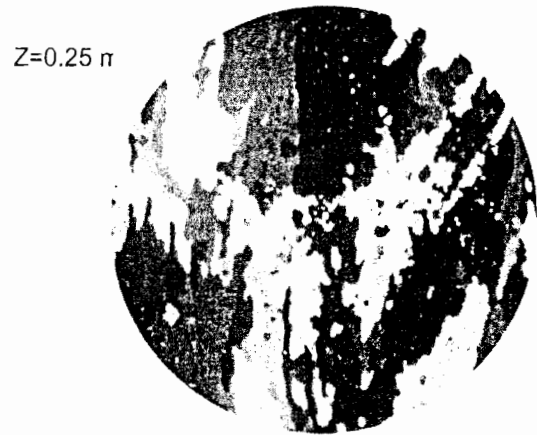
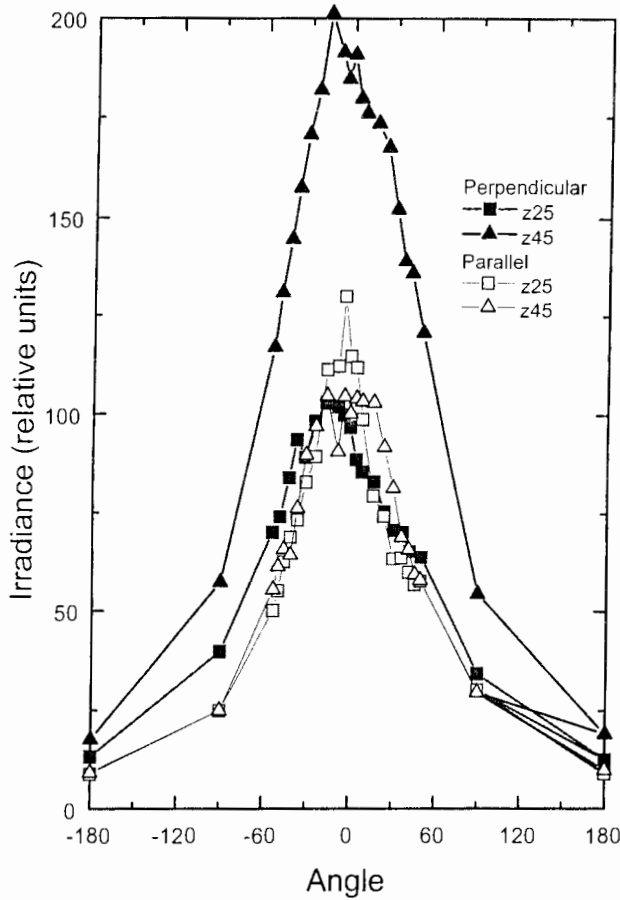
Given the attenuation values and inclusion absorption coefficients in Fig. 8, along with the absorption values of clear ice provided by Grenfell and Perovich [26], we can calculate the average cosine of the light field, which is defined as the vector irradiance (E) divided by the scalar irradiance (E_0). Mathematically, this works out to the cosine function weighted by the radiance distribution averaged over 4π steradians. The average cosine varies between 0.14 and 0.24 from 461 to 600 nm. Because of the rapidly increasing absorption by ice toward longer wavelengths, the average cosine at 665 nm jumps to 0.54. These results are reasonable given the large ice crystals and low absorption by inclusions that characterize the ice at this location. This value differs from the value predicted using the inherent optical properties and radiative transfer theory [27]. The modeled average cosine is about 0.17 m^{-1} , consistent with a K of 2.4 m^{-1} .

It is of interest to compare the bsf's for the two cases of parallel and perpendicular orientation with the ice c -axis. As previously mentioned, the optical axis of the instrument was oriented parallel to the c -axis on May 6 and perpendicular to the c -axis on May 7. Because the data taken for the two orientations were not made on exactly the same volume of sea ice, and were taken on two different days, it is not accurate to compare the peak amplitudes. This is because the peak amplitudes are highly sensitive to local variations in ice structure as well as beam alignment and other sources of error. The widths of the bsf's (ω), which in essence are normalized, should be less sensitive to these factors and thus more confidently compared. Results for the two depths that can be directly compared, namely, 25 and 45 cm, are plotted in

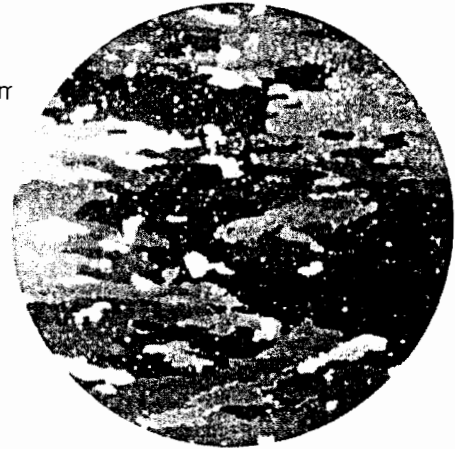
Fig. 9. The bsf width is noticeably larger for the perpendicular orientation compared with the parallel orientation. In other words, light propagation *along* the ice crystal orientation appears to cause higher scattering than light propagation *across* the plane of the ice crystals. Although there is no clear explanation for this effect, the differences in ω are possibly due to differences in the volumes of ice that were measured, and not the orientation of the optical axis. While the areas where the bsf's were measured for both cases were in relatively close proximity, there is evidence to suggest that brine pocket and bubble densities vary significantly over small spatial scales relevant to optical propagation. This might explain the systematic differences in ω . However, there is the possibility that the degree of scattering in ice is significantly affected by the direction of propagation relative to the c -axis in the manner indicated by the bsf data. More work is needed to resolve this issue.

E. Horizontal Variability in Signatures

While much of our effort was directed at examining the electromagnetic properties at specific locations, we also investigated horizontal variability in electromagnetic signatures. In particular, spectral albedos and microwave emissivities were measured every 0.5 m along a 15-m transect. These measurements were first made for the snow-covered ice, after which the snow cover was removed and the measurements were repeated for bare ice. For the snow-covered ice, spectral and wavelength-integrated albedos showed little variation along the transect. While the snow depth varied from 0.07 to 0.14 m along the transect, this did not affect the albedo because the



$Z=0.55 \text{ m}$



0.01 m

Fig. 9. Comparison of bsf's, measured parallel and perpendicular to the c -axis orientation of the ice crystals.

snow was optically thick in all cases. The variability in albedo increased for bare ice, with fluctuations in albedo of $\pm 10\%$ along the transect. The changes in albedo were directly related to small-scale variability in the physical properties of the upper ice layer. Larger albedos were associated with bubbly surface ice layers, while smaller albedos were associated with fewer bubbles, and in some cases, the presence of sediments in the ice [28].

Fig. 10 shows passive microwave emissivity (ϵ) versus position along the same line as the albedo with the natural snow cover in place and later with the snow removed. The observations were taken for five microwave frequencies at both V-pol and H-pol at nadir. Concurrent observations were also made in the thermal infrared (TIR) in the 8-14- μm band. All observations were at a nadir angle of 50° .

For the snow-covered case, the surface emissivity was quite homogeneous except at 90 GHz. The small variations at the lower frequencies were probably due to horizontal inhomogeneities in the near-surface brine volume. The variations at 90 GHz were due primarily to differences in the snow grain size in the sense that the emissivity decreased with increasing grain size. Note that the variations in snow grain size were not sufficiently large to appreciably modify the

spectral albedo. Microwave emissivity is considerably more sensitive to grain size because the sizes found in natural snow are slightly smaller than the observational wavelengths so that the scattering falls between the Rayleigh regime and the geometric optics regime and depends strongly on the size parameter. In the visible and near infrared, the dependence of albedo on grain size for an optically thick snow layer is due to changes in the absorption coefficient of pure ice.

IV. CONCLUSIONS

An interdisciplinary, integrated approach was a central element of this experiment. It allowed us to interpret the electromagnetic results and to relate, at least in a qualitative sense, the variations in electromagnetic properties of sea ice to changes in the state and structure of the snow and ice. Horizontal variability in brightness temperature and backscatter were assessed and related to snow properties. Small-scale changes in albedo were found to be related to surface layer conditions, including air bubbles and particulate levels. There was a large amount of vertical variability in the scattering of visible light that was associated with changes in the size and orientation of the ice crystals and in the number of brine and air inclusions. In the surface layer, where there were numerous inclusions and

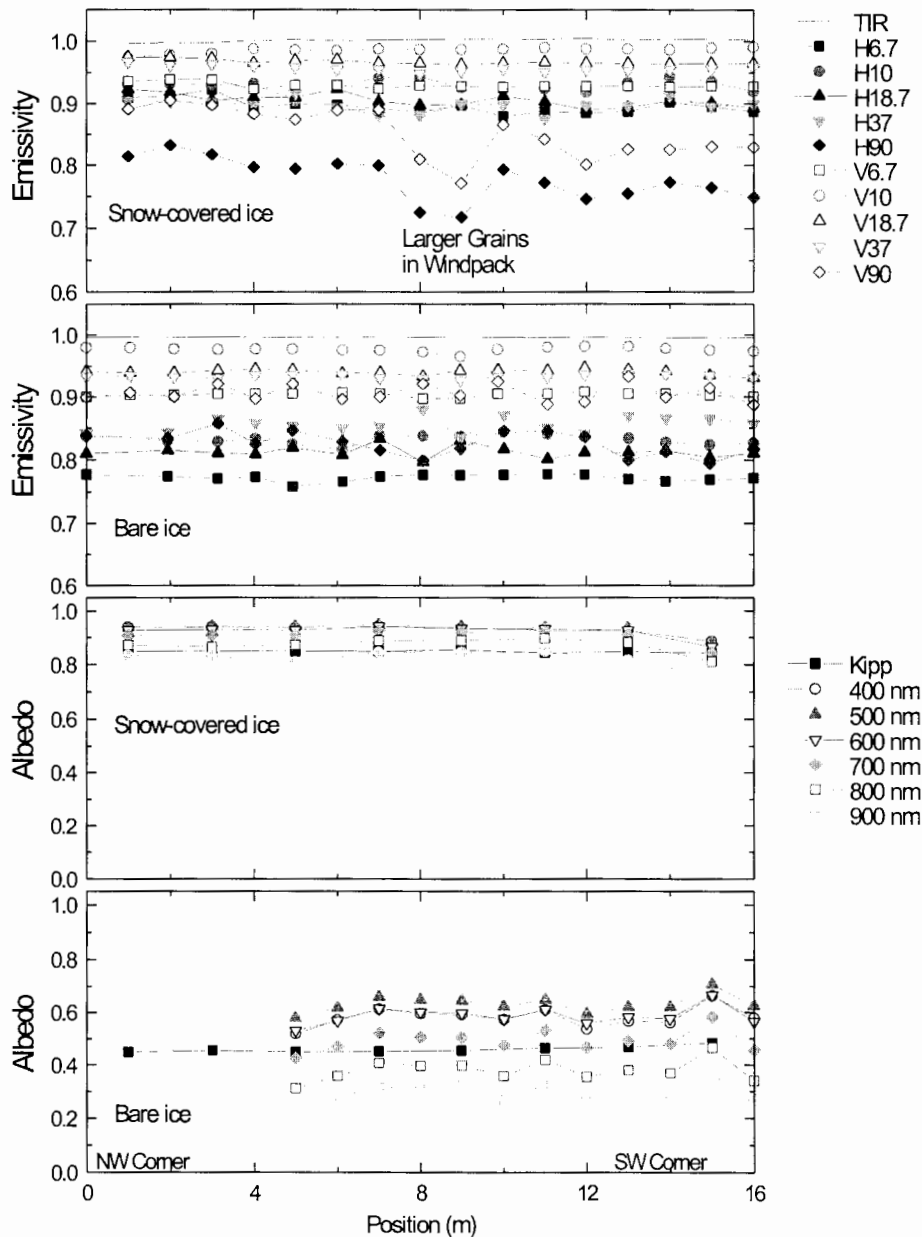


Fig. 10. Horizontal variability of microwave emissivity and albedo for snow-covered and bare first-year ice at selected wavelengths.

crystals tended to be small and randomly oriented, scattering and radiance attenuation were found to be greater.

These combined observations of ice physical and electromagnetic properties provide an excellent resource for model development. Results from this work have already been applied in sea ice radiative transfer modeling efforts [27] and have great potential for further contributions.

This effort represents only a first step in interdisciplinary field studies of the electromagnetic properties of sea ice. More work is needed exploring the effect of crystal orientation on light scattering in sea ice. Similar interdisciplinary experiments examining temporal evolution of electromagnetic signatures during the onset of summer melt are of particular value. Such a study could investigate how changes in the physical state of the ice brought on by melting are reflected in changes in its electromagnetic properties. In addition, relationships between

changes in the microwave and optical signatures could be explored. Finally, an investigation of multiyear ice is needed as this work considered only first-year ice.

ACKNOWLEDGMENT

The efforts of R. Glenn and the staff of Barrow Technical Services were instrumental to the success of the field experiment. The authors thank B. Elder and J. Govoni for their able assistance.

REFERENCES

- [1] W. B. Tucker, III, T. C. Grenfell, R. G. Onstott, D. K. Perovich, A. J. Gow, and R. A. Shuchman, "Microwave and physical properties of sea ice in the winter marginal ice zone," *J. Geophys. Res.*, vol. 96, pp. 4573–4589, 1991.

- [2] W. B. Tucker, III, D. K. Perovich, A. J. Gow, W. F. Weeks, and M. R. Drinkwater. "Chapter 2: Physical properties of sea ice relevant to remote sensing," in *Microwave Remote Sensing of Sea Ice*. Washington, DC: Amer. Geophys. Union, 1992, p. 462.
- [3] K. C. Jezek, D. K. Perovich, K. M. Golden, C. Luther, D. G. Barber, P. Gogineni, T. C. Grenfell, A. K. Jordan, C. D. Mobley, S. V. Nghiem, and R. G. Onstott. "A broad spectral, interdisciplinary investigation of the electromagnetic properties of sea ice," this issue, pp. 1633–1641.
- [4] T. C. Grenfell, D. G. Barber, A. K. Fung, A. J. Gow, K. C. Jezek, E. J. Knapp, S. V. Nghiem, R. G. Onstott, D. K. Perovich, C. S. Roesler, C. T. Swift, and F. Tanis. "Evolution of electromagnetic signatures of sea ice from initial formation to the establishment of thick first-year ice," this issue, pp. 1642–1654.
- [5] D. G. Barber, S. P. Reddan, and E. F. LeDrew. "Statistical characterization of the geophysical and electrical properties of snow on landfast first-year sea ice." *J. Geophys. Res.*, vol. 100, no. C2, pp. 2673–2686, 1994.
- [6] A. Assur. "Composition of sea ice and its tensile strength" in *Arctic Sea Ice*. U.S. Nat. Acad. Sci., Nat. Res. Council, Publ. 598, 1958, pp. 106–138.
- [7] G. Frankenstein and R. Garner. "Equations for determining the brine volume of sea ice from -0.5 – 22.9 °C," *J. Glaciol.*, vol. 6, pp. 943–944, 1967.
- [8] G. F. N. Cox and W. F. Weeks. "Equations for determining the gas and brine volumes in sea ice," *J. Glaciol.*, vol. 12, pp. 309–316, 1983.
- [9] W. B. Tucker, III, A. J. Gow, and W. F. Weeks. "Physical properties of summer sea ice in the Fram Strait," *J. Geophys. Res.*, vol. 92, pp. 6787–6803, 1987.
- [10] A. Bricaud, L. Priur, and A. Morel. "Absorption by dissolved organic matter of the sea (yellow substance) in the UV and visible domains," *Limnol. Oceanogr.*, vol. 26, pp. 43–53, 1981.
- [11] B. G. Mitchell. "Algorithms for determining the absorption coefficient of aquatic particulates using the quantitative filter technique (QFT)," in *Proc. SPIE Int. Soc. Opt. Eng. Ocean Opt.*, 1990, vol. 10, no. 1302, pp. 137–148.
- [12] C. S. Roesler and M. J. Perry. "In situ phytoplankton absorption, fluorescence emission, and particulate backscattering spectra determined from reflectance," *J. Geophys. Res.*, vol. 100, no. 13, p. 279, 1995.
- [13] C. S. Roesler. "Retrieval of particulate absorption coefficients from the quantitative filter technique: A radiative transfer approach to quantifying pathlength amplification," submitted for publication.
- [14] C. S. Roesler and R. Iturriaga. "Absorption properties of marine-derived material in Arctic sea ice," in *Proc. SPIE Int. Soc. Opt. Eng. Ocean Opt.*, 1994, vol. 12, no. 2258, pp. 933–943.
- [15] C. S. Roesler and R. L. Hansing. "Analysis of particle concentrations and size distributions in fresh and marine waters," submitted for publication.
- [16] O. Holm-Hansen, C. J. Lorenzen, R. W. Holmes, and J. D. H. Strickland. "Fluorometric determination of chlorophyll," *J. Cons. Int. Explor. Mer.*, vol. 30, pp. 3–15, 1965.
- [17] D. K. Perovich. "Light reflection from sea ice during the onset of melt," *J. Geophys. Res.*, vol. 99, pp. 3351–3359, 1994.
- [18] R. A. Maffione and C. D. Mobley. "Theory and measurements of the complete beam spread function of sea ice," *Limnol. Oceanogr.*, to be published.
- [19] D. G. Barber, A. K. Fung, T. C. Grenfell, S. V. Nghiem, R. G. Onstott, V. I. Lytle, D. K. Perovich, and A. J. Gow. "The role of snow on microwave emission and scattering over first-year sea ice," this issue, pp. 1750–1763.
- [20] D. K. Perovich and T. C. Grenfell. "Laboratory studies of the optical properties of young sea ice," *J. Glaciol.*, vol. 27, pp. 331–346, 1981.
- [21] T. C. Grenfell and G. A. Maykut. "The optical properties of ice and snow in the Arctic basin," *J. Glaciol.*, vol. 18, pp. 445–463, 1977.
- [22] T. C. Grenfell and D. K. Perovich. "Spectral albedos of sea ice and incident solar irradiance in the southern Beaufort Sea," *J. Geophys. Res.*, vol. 89, pp. 3573–3580, 1984.
- [23] D. K. Perovich. "Observations of ultraviolet light reflection and transmission by first-year sea ice," *Geophys. Res. Lett.*, vol. 22, pp. 1349–1352, 1995.
- [24] R. G. Onstott. "Chapter 5: SAR and scatterometer signatures of sea ice," in *The Remote Sensing of Sea Ice*. Washington, DC: Amer. Geophys. Union, 1992, p. 462.
- [25] D. K. Perovich, G. F. Cota, G. A. Maykut, and T. C. Grenfell. "Bio-optical observations of first-year Arctic sea ice," *Geophys. Res. Lett.*, vol. 20, pp. 1059–1062, 1993.
- [26] T. C. Grenfell and D. K. Perovich. "Radiation absorption coefficients of polycrystalline ice from 400–1400 nm," *J. Geophys. Res.*, vol. 86, pp. 7447–7450, 1981.
- [27] C. D. Mobley, G. F. Cota, T. C. Grenfell, R. A. Maffione, W. S. Pegau, and D. K. Perovich. "Modeling light propagation in sea ice," this issue, pp. 1743–1749.
- [28] C. S. Roesler and R. G. Onstott. "Organic material entrapped in arctic sea ice: The influence on the optical, thermal and physical properties of arctic sea ice," submitted for publication.

Donald K. Perovich, for a photograph and biography, see p. 124 of the January 1998 issue of this TRANSACTIONS.

Jacob Longacre, photograph and biography not available at the time of publication.

David G. Barber, for a photograph and biography, see p. 50 of the January 1998 issue of this TRANSACTIONS.

Robert A. Maffione, photograph and biography not available at the time of publication.

Glenn F. Cota, photograph and biography not available at the time of publication.

Curtis D. Mobley, photograph and biography not available at the time of publication.

Anthony J. Gow, for a photograph and biography, see p. 124 of the January 1998 issue of this TRANSACTIONS.

Robert G. Onstott (S'73–M'79), photograph and biography not available at the time of publication.

Thomas C. Grenfell (M'94–A'95), for a photograph and biography, see p. 124 of the January 1998 issue of this TRANSACTIONS.

W. Scott Pegau, photograph and biography not available at the time of publication.

Mark Landry, photograph and biography not available at the time of publication.

Collin S. Roesler, photograph and biography not available at the time of publication.